Nanoscale

Accepted Manuscript

This article can be cited before page numbers have been issued, to do this please use: Y. Lee, W. Choi, S. Woo, Y. Cho, G. Lim, J. Joo, K. R. Han, I. W. Cheong, D. Lee, J. Choi and P. J. Kim, *Nanoscale*, 2026, DOI: 10.1039/D6NR01899H.

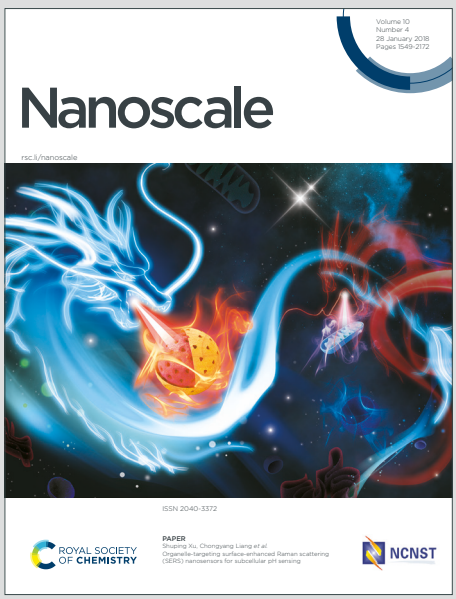

ROYAL SOCIETY OF CHEMISTRY

rsc.li/nanoscale

View Article Online
DOI: 10.1039/D5NR01899H

Submicron Interfacial Layers for Nanoscale Control of Lithium Deposition in Surface-Engineered Current Collectors

Received 00th January 20xx,
Accepted 00th January 20xx

DOI: 10.1039/x0xx00000x

Yujin Lee[a,†], Wootaek Choi[a,†], Sujeong Woo[b], Yeonseo Cho[a], Geunah Lim[b], Jin Joo[b], Kyung Rok Han[b], In Woo Cheong[b], Dongsoo Lee[c], Junghyun Choi[c*], and Patrick Joohyun Kim[a,b*]*

Lithium metal batteries (LMBs) have garnered considerable attention owing to their high theoretical capacity and low electrochemical potential; however, their practical implementation is hindered by unstable Li plating/stripping and poor interfacial stability. Previous strategies have largely focused on enhancing lithiophilicity or wettability to regulate initial Li deposition, yet they do not necessarily ensure stable long-term cycling. In this study, an interfacial buffer layer was rationally designed for metal-based current collectors to elucidate the distinct contributions of lithiophilicity and wettability to Li deposition behavior. A comparison of representative material systems designed to decouple these effects revealed that interfacial stability, derived from mechanical robustness and adhesion, governs long-term electrochemical performance. Bare Cu induces localized Li nucleation and forms a compositionally heterogeneous and unstable solid electrolyte interphase (SEI), leading to dendritic growth and dead Li accumulation. Conversely, a graphene oxide–poly(vinylidene fluoride)-coated current collector enables uniform Li deposition and promotes the formation of a mechanically robust and chemically homogeneous SEI, improving plating/stripping reversibility. The submicron-thick coating enables effective interfacial control without compromising practical electrode configurations. The resulting system delivers a stable Coulombic efficiency of ~75% over 120 cycles, whereas other configurations exhibit rapid degradation due to interfacial instability. XPS depth profiling revealed the formation of a uniform and lithium fluoride(LiF)-rich SEI with minimal depth-dependent variation, indicating a stabilized interphase. These findings highlight that long-term stability in LMBs is governed by mechanically robust interfacial stability during repeated cycling rather than by initial nucleation behavior, providing clear design guidelines for interface-engineered current collectors.

Introduction

Rechargeable batteries are widely utilized across diverse energy storage applications.[1] However, the energy density of conventional lithium-ion batteries is limited, necessitating the development of high-capacity anode materials.[2] Lithium metal (Li) is considered a promising candidate for next-generation anodes owing to its high theoretical capacity and low electrochemical potential.[3-5] Despite these advantages, its practical implementation is hindered by unstable Li plating/stripping and poor electrochemical reversibility.[6, 7] During repeated cycling, non-uniform Li deposition occurs on the current collector, leading to dendritic growth and the formation of electrically isolated dead Li, which collectively accelerate electrolyte decomposition.[8-10] These parasitic reactions result in irreversible Li consumption and ultimately limit the cycle life of the battery.[11, 12]

To address these intrinsic challenges, various strategies have been extensively explored to regulate Li deposition behavior and stabilize the electrode–electrolyte interface.[13] Among them, surface modification of current collectors has emerged as an effective strategy for controlling Li nucleation and growth.[14, 15] In particular, the introduction of lithiophilic layers reduces nucleation overpotential and promotes homogeneous Li nucleation during the initial stages of cycling, thereby suppressing the localized growth that triggers dendrite formation.[16-18] In addition, interfacial engineering strategies, such as defect engineering and the incorporation of artificial interlayers, have been explored to further modulate interfacial behavior and improve cycling performance.[19, 20]

However, most existing strategies primarily focus on initial Li nucleation and do not adequately address interfacial stability during prolonged cycling.[21] Repeated Li plating and stripping induce substantial volume fluctuations, which generate mechanical stress at the interface between the current collector and the coating layer.[22, 23] Consequently, Li gradually accumulates in specific regions, resulting in non-uniform morphologies and dendritic growth.[24] These observations suggest that uniform initial nucleation alone is insufficient to ensure stable long-term cycling.[25, 26]

Moreover, properties traditionally regarded as beneficial, such as enhanced wettability, do not necessarily correlate with improved long-term electrochemical performance.[27-29] Although increased wettability can facilitate electrolyte infiltration and improve initial interfacial contact, it does not

[a] School of Semiconductor Convergence Engineering, Kyungpook National University, Daegu, 41566, Korea; pjkim@knu.ac.kr.
[b] School of Chemical Engineering and Applied Chemistry, Kyungpook National University, Daegu, 41566, Korea.
[c] School of Chemical, Biological and Battery Engineering, Gachon University, Seongnam-si, Gyeonggi-do 13120, Republic of Korea. E-mail: dslee9117@gachon.ac.kr; junghchoi@gachon.ac.kr.
† These authors contributed equally to this work.
*Corresponding Author

View Article Online
DOI: 10.1039/D6NR01899H

guarantee sustained interfacial stability under repeated cycling.[28, 30, 31] Thus, long-term electrochemical performance is governed by interfacial stability rather than initial interfacial affinity.[32, 33] These considerations highlight the necessity for a systematic framework to decouple and understand the individual contributions of key interfacial properties.

In this study, an interfacial buffer layer was rationally designed for metal-based current collectors to elucidate the respective roles of lithiophilicity and wettability in Li deposition behavior. The designed layer comprises a submicron-thick carbon-based coating that enables effective interfacial regulation while maintaining practical feasibility for scalable battery systems. To decouple these effects, two representative material systems were employed. Graphene (Gr) and grapheneoxide (GO) were selected to differentiate wettability-dominant and lithiophilicity-dominant characteristics, respectively, while poly(vinylidene fluoride) (PVDF) and poly(acrylic acid) (PAA) binders were used to compare interfacial adhesion and electrolyte wettability.[34-36] Specifically, Gr exhibits lithiophilic behavior upon interaction with Li, whereas GO provides enhanced wettability due to its oxygen-containing functional groups despite its limited intrinsic lithiophilicity.[24, 37, 38] Similarly, PAA offers high wettability but suffers from limited interfacial stability due to swelling, whereas PVDF forms a more mechanically robust and well-adhered interface despite its lower wettability.[39-41] Within this framework, the combination of GO and PVDF is expected to provide a uniform and mechanically stable interfacial layer, facilitating the formation of a homogeneous SEI layer that regulates Li-ion flux and suppresses localized deposition.[42]

Li||Cu half-cell configurations were electrochemically evaluated. It was discovered that systems with high initial lithiophilicity or wettability exhibit improved early-stage Li deposition but undergo performance degradation during prolonged cycling due to insufficient interfacial stability. Conversely, coating layers that provide strong adhesion and mechanical robustness maintain stable cycling behavior, effectively suppressing dendritic growth and minimizing dead Li formation.[43] These findings collectively indicate that interfacial stability, rather than initial interfacial affinity, plays a critical role in long-term electrochemical performance, highlighting the importance of mechanically robust and well-adhered interfacial layers for durable LMBs.

Experimental

Fabrication of Gr–PVDF, GO–PVDF, and GO–PAA

Gr (multilayer flakes, C-1, Graphene Supermarket) and GO (GO-V20, Standard Graphene) were used as surface-modifying materials. Slurries were prepared by mixing Gr or GO with polymer binder solutions at a mass ratio of 9:1. The binder solutions consisted of 6 wt% PVDF dissolved in 1-methyl-2-pyrrolidone (NMP; 99.5%, SAMCHUN) or 10 wt% PAA in deionized water. The mixtures were homogeneously dispersed using a planetary mixer (AR-100, THINKY). The resulting slurries were cast onto copper foil using a doctor blade and subsequently dried in a convection oven at 50 °C overnight. Thereafter, the dried electrodes were punched into circular disks (12 mm in diameter).

Characterization

The chemical structures of Gr and GO were characterized using Raman spectroscopy, FT-IR spectroscopy, and elemental analysis. The Raman spectra were acquired using an inVia Reflex (Renishaw) with a 532 nm laser, whereas FT-IR measurements were performed using a Frontier spectrometer (PerkinElmer) in the range of 400–4000 cm^{-1}. Elemental analysis was conducted using a FlashSMART analyzer (Thermo Fisher Scientific). To evaluate surface polarity, contact angle measurements were performed using deionized water as a probe liquid (Phoenix 300, SEO). The morphologies of the current collectors were examined via field-emission scanning electron microscopy (FE-SEM; SU8220, Hitachi), and additional surface characterization was achieved using atomic force microscopy (AFM; XE7, Park Systems). The chemical composition of the electrode surfaces was analyzed using X-ray photoelectron spectroscopy (XPS; Nexsa, Thermo Fisher Scientific). For the XPS analysis, the cells were disassembled in an argon-filled glovebox, and the electrodes were transferred to a vacuum holder to minimize air exposure. Depth profiling was performed using Ar sputtering at different etching times (0 and 60 s).

Electrochemical measurements

Electrochemical performance was evaluated using CR2032-type coin cells assembled in an argon-filled glovebox, where the O_2 and H_2O concentrations were maintained below 0.1 ppm. Each cell consisted of a Li metal foil (0.6 mm thick) and a polypropylene separator (Celgard 2400, 18 mm diameter). The electrolyte was 1.0 M $LiPF_6$ dissolved in a mixture of ethylene carbonate and diethyl carbonate (1:1 vol%, Enchem). Galvanostatic cycling was conducted using a battery tester (CT-4008Q-5 V100 mA-124, Neware). Electrochemical impedance spectroscopy (EIS) measurements were conducted using a potentiostat (SP-150e, Bio-Logic, France) over a frequency range of 10 mHz to 200 kHz with an AC amplitude of 10 mV.

Results and discussion

Although uniform initial Li nucleation and improved wettability are generally considered beneficial, they do not inherently ensure interfacial structural stability during repeated cycling and therefore do not guarantee enhanced long-term electrochemical performance.[28] Fig. 1 schematically illustrates the influence of the bare Cu and GO–PVDF on Li nucleation and growth behavior.

Bare Cu is inherently lithiophobic, resulting in localized Li nucleation at limited surface sites.[36] This initial non-uniformity becomes progressively amplified over repeated cycles, leading to uncontrolled, heterogeneous, and dendritic Li growth.[44] Concurrently, the SEI formed via electrolyte decomposition exhibits chemical and mechanical instability, along with poor

View Article Online
DOI: 10.1039/D6NR01899H

adhesion to the deposited Li. As a result, portions of the deposited Li become detached from the current collector during stripping, forming electrically isolated dead Li that no longer participates in subsequent electrochemical reactions.[45] These processes collectively reduce the reversibility of Li plating/stripping and lead to degraded long-term electrochemical performance.

In contrast, the GO–PVDF creates a more favorable interfacial environment for Li deposition. The GO layer, enriched with oxygen-containing functional groups, promotes uniform interactions with Li^+ ions, resulting in spatially homogeneous Li nucleation across the surface.[46] This uniformity is preserved throughout subsequent cycling, enabling more controlled Li growth. Furthermore, the GO–PVDF coating facilitates the formation of a uniform and mechanically robust SEI layer, which maintains strong interfacial adhesion and structural stability during repeated Li plating and stripping. Such a stable SEI effectively suppresses Li detachment and mitigates the formation of electrically isolated dead Li.[45] This significantly improves the reversibility of Li plating/stripping, leading to enhanced long-term electrochemical performance.[47]

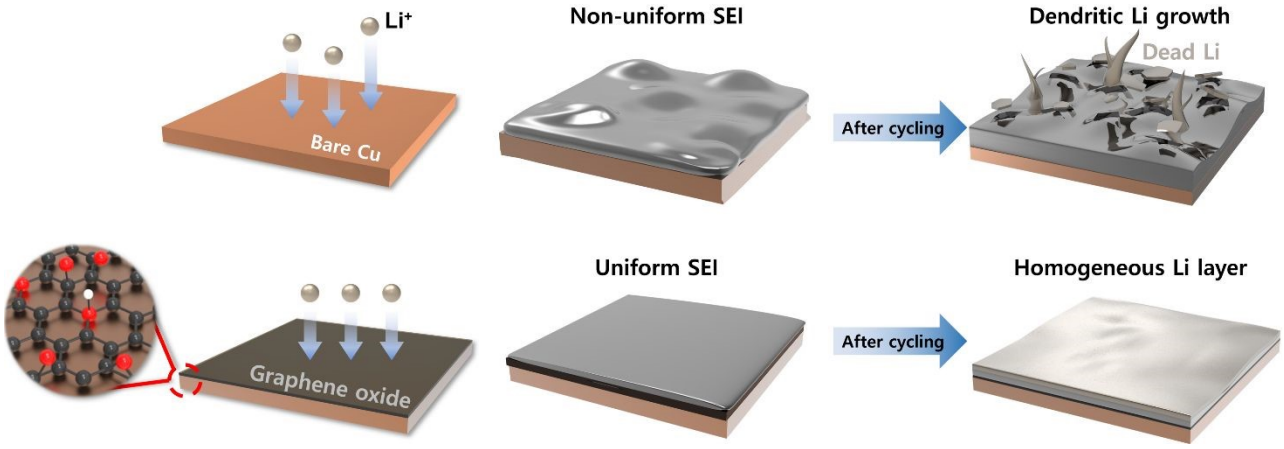

Fig. 1 Schematic illustration comparing Li nucleation and growth on bare Cu and GO–PVDF. Bare Cu induces localized nucleation, leading to dendritic growth, unstable SEI formation, and dead Li accumulation after cycling. In contrast, GO–PVDF enables uniform nucleation and the formation of a robust SEI, suppressing dendrite growth and improving reversibility.

Fig. 2a presents the fabrication process for Gr–PVDF, GO–PAA, and GO–PVDF, wherein Gr and GO slurries are cast onto bare Cu via a tape-casting process to form uniform coating layer. As shown in Fig. 2b, all samples exhibited continuous and homogeneous coverage over the Cu surface. Notably, the coating exhibited a submicron-scale thickness and an average mass loading of approximately 0.047 mg cm^{-2}, enabling effective interfacial modification while maintaining the original current collector structure.

The collected Raman spectra displayed an increased D/G intensity ratio for GO (Fig. 2c), indicating a higher defect density and partial disruption of the sp^2 carbon network due to the introduction of oxygen-containing functional groups.[48] FT-IR analysis further confirmed the presence of O–H, C=O, and C–O bonds (Fig. 2d), which correspond to hydroxyl, carbonyl, and carboxyl groups.[37] Consistently, the elemental analysis results revealed a significant increase in the oxygen content in GO (Fig. 2e), which suggests a higher density of active sites for Li^+ interaction.[46] These compositional changes are also expected to increase surface polarity.

To evaluate the effect of surface polarity, contact angle measurements were performed using a polar solvent, i.e., deionized water (Fig. 2f–i). The bare Cu exhibited a contact angle of ~90°, indicating relatively poor wettability. Gr–PVDF displayed a higher contact angle (~112°), reflecting its hydrophobic nature. In contrast, the GO-based coatings, GO–PVDF (~73°) and GO–PAA (~52°), exhibited significantly reduced contact angles, demonstrating enhanced wettability. These results indicate that the oxygen-containing functional groups in GO increase surface polarity and electrolyte wettability.[49] Such enhanced affinity is expected to facilitate uniform Li-ion distribution at the interface during the initial stage of deposition.[24]

The surface morphology was examined using SEM at both low and high magnifications (Fig. 2j–q). All coatings uniformly covered the bare Cu surface without noticeable agglomeration, effectively masking the original surface features. The GO-based coatings exhibited a wrinkled morphology, whereas the Gr-based coatings displayed a flake-like structure.[50, 51] AFM analysis (Fig. S1) further confirmed that the characteristic linear texture of bare Cu disappeared after coating, indicating the formation of a continuous and conformal overlayer.

View Article Online
DOI: 10.1039/D6NR01899H

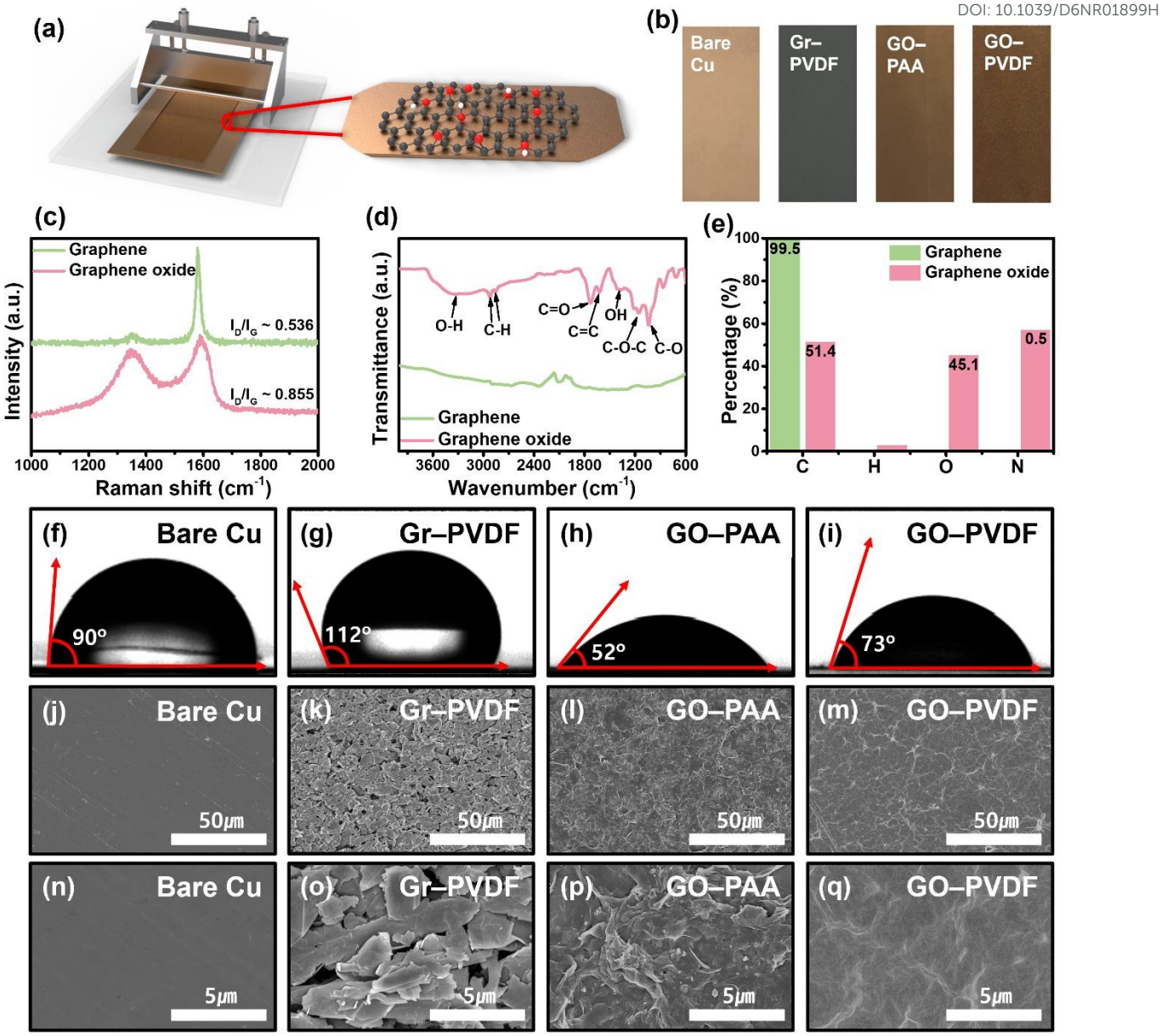

Fig. 2 (a) Schematic illustration of the fabrication process for each current collector. (b) Photograph of the prepared samples. (c) Raman spectra, (d) FT-IR spectra, and (e) elemental analysis results of the Gr and GO powders. Contact angle images of (f) bare Cu, (g) Gr–PVDF, (h) GO–PAA, and (i) GO–PVDF. Top-view SEM images of the samples at (j–m) low magnification and (n–q) high magnification.

The interfacial adhesion and structural stability of the coating layers were evaluated through a peel-off test, as illustrated in Fig. 3a. A small amount of organic electrolyte was applied to the coated current collectors, and then a tape was attached and subsequently removed. The peeled regions were analyzed to assess the integrity of the remaining coating layers.

For Gr–PVDF, the electrolyte spread extensively across the surface (Fig. 3e), likely due to infiltration through the voids within the flake-like graphene structure. After the peel-off test, most of the coating layer was removed (Fig. 3h), indicating weak interfacial adhesion to the Cu substrate. SEM analysis further confirmed that only a limited amount of the coating remained (Fig. 3k), which resulted in discontinuous surface coverage.

In the case of GO–PAA, the electrolyte spread rapidly over the surface (Fig. 3f), which can be attributed to the hydrophilic functional groups in PAA that enhance electrolyte affinity.[39] Although the coating layer was not completely removed after the peel-off test, significant electrolyte penetration likely induced swelling and structural disruption (Fig. 3i). Such electrolyte infiltration facilitates internal swelling and stress accumulation within the coating layer, ultimately leading to interfacial delamination and structural degradation.[52] This compromised structural stability is corroborated by the SEM images, which revealed pronounced deformation of the surface morphology (Fig. 3l).

In contrast, the GO–PVDF exhibited markedly different behavior. The electrolyte remained as discrete droplets without noticeable spreading (Fig. 3g), indicating limited electrolyte infiltration into the coating layer. After the peel-off test, the coating remained intact with no observable damage (Fig. 3j).

View Article Online
DOI: 10.1039/D6NR01899H

The SEM images confirmed that the characteristic wrinkled morphology of GO was well preserved (Fig. 3m), demonstrating robust structural integrity. Based on a qualitative comparison, GO–PVDF exhibits the strongest adhesion, followed by GO–PAA and Gr–PVDF.

These results indicate that the GO–PVDF provides strong interfacial adhesion and mechanical stability, effectively resisting electrolyte-induced degradation. Such stable interfacial characteristics are anticipated to play a critical role in regulating Li deposition behavior and enhancing long-term cycling stability.[53] In particular, the mechanically robust and well-adhered GO–PVDF is expected to facilitate the formation of a uniform and stable SEI, which can suppress localized Li-ion flux and mitigate the formation of dendritic Li and dead Li during repeated cycling. This suggests that interfacial adhesion, rather than wettability alone, is a key factor in maintaining interfacial integrity under electrolyte exposure.

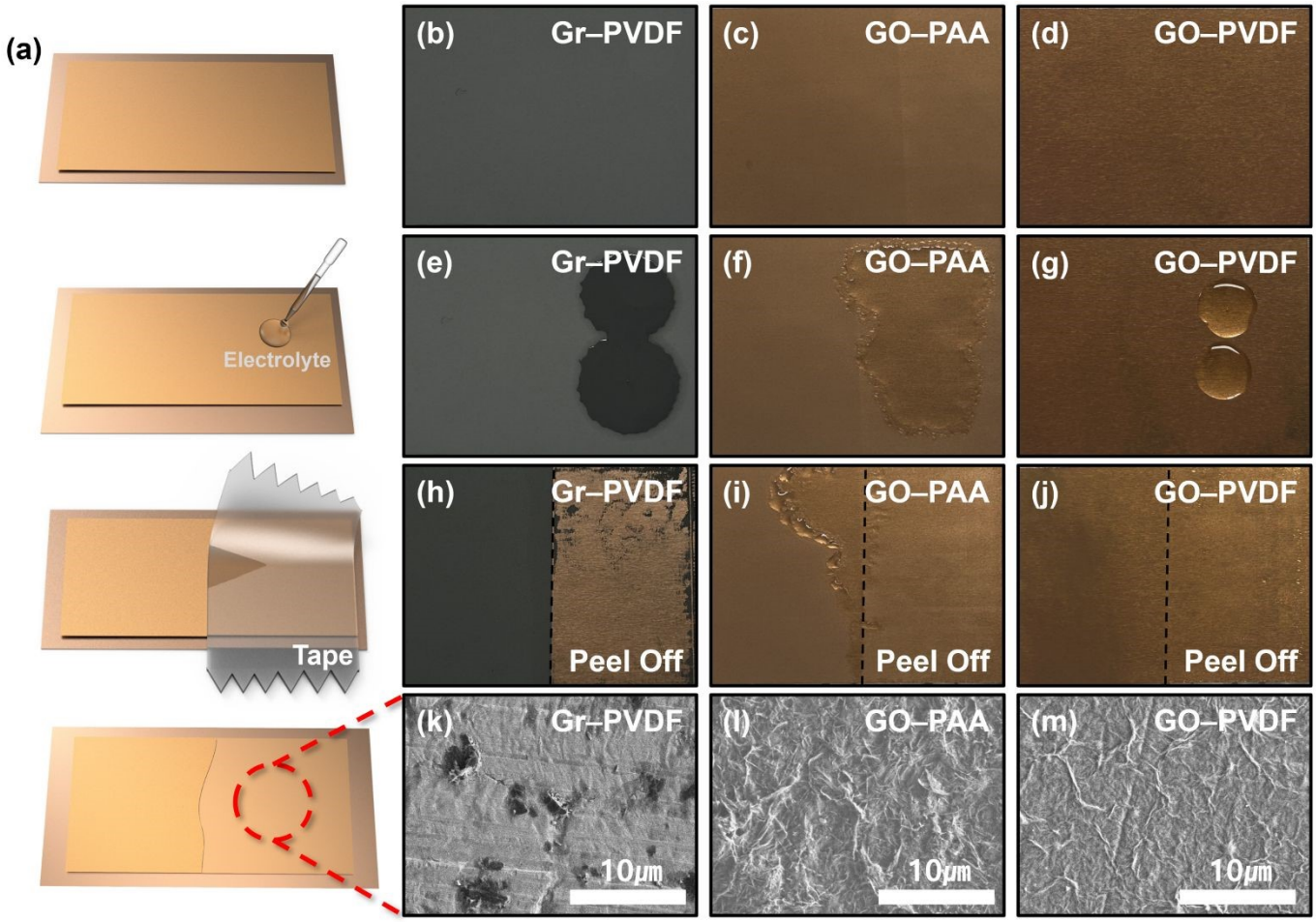

Fig. 3 (a) Schematic illustration of the peel-off test procedure. (b–d) Optical images of pristine Gr–PVDF, GO–PAA, and GO–PVDF. (e–g) Optical images of the samples after electrolyte droplet deposition. (h–j) Optical images and (k–m) top-view SEM images of Gr–PVDF, GO–PAA, and GO–PVDF after the peel-off test.

View Article Online
DOI: 10.1039/D6NR01899H

Li plating/stripping tests were conducted to elucidate how the interfacial characteristics of the Gr– and GO–based coatings influence Li deposition behavior. Fig. 4a presents the cycling performance of Li||Cu cells employing the bare Cu, Gr–PVDF, and GO–PVDF at a current density of 1.0 mA cm^{-2} and an areal capacity of 1.0 mAh cm^{-2}. While all samples exhibited comparable Coulombic efficiencies during the initial cycles, the Gr–PVDF demonstrated lower initial Coulombic efficiency than bare Cu owing to irreversible Li consumption associated with interfacial reactions between Gr and Li. In the case of GO–PVDF, although two-dimensional GO–based coatings have been reported to exhibit reduced Li^+ diffusion barriers after initial lithiation, Li^+ ions must overcome an additional energy barrier during the initial cycles to establish effective transport pathways within the coating layer, resulting in a slightly reduced initial Coulombic efficiency. [54]

As cycling progressed, the performance differences became more pronounced. Specifically, the bare Cu exhibited a sharp decline in Coulombic efficiency after approximately 30 cycles, which is attributed to interfacial instability and dead Li formation induced by non-uniform Li deposition. Gr–PVDF initially maintained a relatively stable Coulombic efficiency, which gradually decreased after around 40 cycles. This behavior is consistent with the peel-off test results, indicating that insufficient interfacial adhesion and structural instability of the coating layer lead to progressive interfacial degradation. Repeated Li plating/stripping induces volume changes that generate mechanical stress at the interface, eventually causing cracking, delamination, and loss of interfacial contact. These effects promote localized Li deposition, heterogeneous growth, and dendritic Li formation, thereby accelerating irreversible Li consumption and reducing the Coulombic efficiency.

In contrast, GO–PVDF maintained a stable Coulombic efficiency of ~75% even after 120 cycles. This enhanced stability can be attributed to the GO-based layer, which preserves strong interfacial adhesion and structural integrity, thereby enabling a uniform Li-ion flux and effectively suppressing localized Li deposition. The submicron-scale architecture enables interfacial stabilization without introducing significant transport resistance or mass penalty, thereby contributing to sustained electrochemical performance. This behavior is further corroborated by the voltage profiles (Fig. 4b–d). During the initial cycle, Gr–PVDF and GO–PVDF exhibited similar nucleation overpotentials. However, their long-term stability diverged significantly with cycling. After 50 and 100 cycles, both bare Cu and Gr–PVDF displayed increasingly unstable voltage profiles with reduced reversibility, whereas GO–PVDF retained a voltage response comparable to that observed during the initial cycle, indicating sustained reversible Li plating/stripping.

Similar trends were observed under milder conditions of 0.5 mA cm^{-2} and 0.5 mAh cm^{-2} (Fig. 4e). GO–PVDF maintained relatively high Coulombic efficiency and stable cycling performance, while bare Cu and Gr–PVDF exhibited gradual degradation. Notably, this performance gap persisted even under a reduced current density and capacity, underscoring the dominant role of interfacial stability. Under more aggressive conditions of 2 mA cm^{-2} and 2 mAh cm^{-2}, the differences became more pronounced, with GO–PVDF demonstrating superior stability (Fig. 4f).

To evaluate the effect of current density on electrochemical kinetics and reversibility, Li metal cells were tested under stepwise increases in current densities from 0.5 to 1 mA cm^{-2} (Fig. 4g). As the current density increased, all samples exhibited a gradual decrease in Coulombic efficiency, which can be attributed to enhanced Li-ion flux promoting non-uniform interfacial reactions and irreversible Li consumption. Notably, GO–PVDF maintained relatively high Coulombic efficiency even at elevated current densities. Furthermore, when the current density was returned to 1 mA cm^{-2}, GO–PVDF recovered to a Coulombic efficiency close to its initial level, indicating that it effectively preserves interfacial integrity even under high-current conditions. In contrast, bare Cu and Gr–PVDF failed to fully recover their initial Coulombic efficiency, suggesting irreversible interfacial damage and accumulated dead Li formation.

To investigate the evolution of interfacial resistance during cycling, EIS was performed. After the initial cycle, the ohmic resistance (R_{ohmic}) values for bare Cu, Gr–PVDF, and GO–PVDF were 8, 6, and 4 Ω, respectively (Fig. 4h), indicating reduced resistance for the samples. The charge-transfer resistance (R_{ct}) values of bare Cu, Gr–PVDF, and GO–PVDF were 113, 36, and 134 Ω, respectively. The low initial R_{ct} of Gr–PVDF is due to the high electrical conductivity of graphene, which facilitates rapid charge transfer.[55] In contrast, the relatively high initial R_{ct} of GO–PVDF is due to the intrinsically low conductivity of GO.

However, after 100 cycles, distinct differences in resistance evolution emerged (Fig. 4i). The R_{ohmic} for bare Cu, Gr–PVDF, and GO–PVDF increased to 24, 11, and 5 Ω, respectively, while the R_{ct} increased to 381, 175, and 142 Ω. The pronounced increase in the resistance of Gr–PVDF indicates severe interfacial degradation caused by coating delamination and unstable SEI formation. In contrast, the relatively moderate increase in the resistance of GO–PVDF despite its higher initial R_{ct} demonstrates that the GO-based coating effectively stabilizes the interface and suppresses resistance growth by maintaining a uniform and stable SEI. Overall, these results indicate that while initial conductivity influences early-stage kinetics, long-term electrochemical performance is predominantly governed by sustained interfacial integrity during repeated cycling.

View Article Online
DOI: 10.1039/D6NR01899H

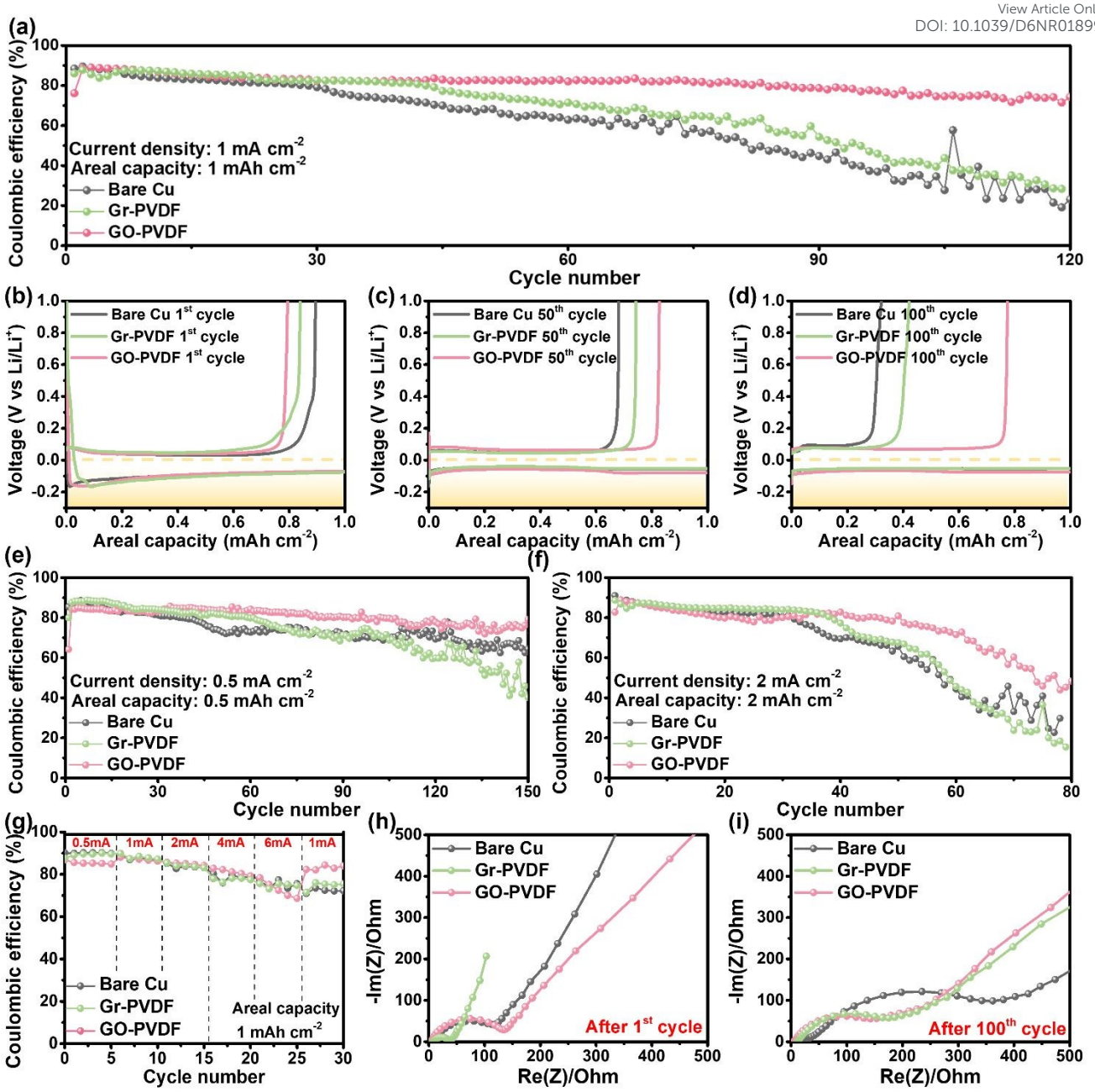

Fig. 4 (a) Cycling performance of Li||Cu half cells employing the bare Cu, Gr–PVDF, and GO–PVDF at a current density of 1.0 mA cm^{-2} and an areal capacity of 1.0 mAh cm^{-2}. (b–d) Galvanostatic charge–discharge profiles at the 1st, 50th, and 100th cycles. Cycling performance at (e) 0.5 mA cm^{-2} with 0.5 mAh cm^{-2} and (f) 2.0 mA cm^{-2} with 2.0 mAh cm^{-2}. (g) Rate capability of the corresponding cells. EIS spectra obtained after (h) the 1st cycle and (i) the 100th cycle.

View Article Online
DOI: 10.1039/D6NR01899H

Improved wettability does not necessarily translate to enhanced long-term electrochemical performance. To investigate this, Li||Cu half-cell tests were conducted using GO-based coatings with two different binders: aqueous PAA and non-aqueous PVDF. Owing to its high polarity and hydrophilicity, PAA facilitates rapid electrolyte infiltration at the initial stage; however, its influence on interfacial stability during prolonged cycling is limited.

As shown in Fig. 5a, GO–PVDF maintained a stable Coulombic efficiency of ~75% over 120 cycles, whereas GO–PAA exhibited a gradual decline in efficiency after approximately 50 cycles, eventually dropping below 20%. This contrast suggests that enhanced wettability alone is insufficient to guarantee long-term electrochemical performance. Although increased wettability promotes initial electrolyte infiltration, it also facilitates the penetration of the electrolyte into the coating layer, leading to swelling and structural deformation during cycling. Such degradation disrupts the continuity and mechanical integrity of the coating, while repeated Li plating/stripping further exacerbates interfacial deformation.[27] Consequently, localized SEI breakdown and reformation occur, accelerating dead Li formation and performance decay. These differences are further reflected in the voltage profiles (Fig. 5b–d). During the initial cycle, both samples exhibited comparable voltage behavior, suggesting similar nucleation characteristics. However, their electrochemical responses diverged significantly as cycling progressed. After 50 and 100 cycles, GO–PAA displayed unstable voltage profiles with increased polarization and fluctuating overpotential, indicating deteriorated interfacial kinetics, whereas GO–PVDF maintained stable and reproducible behavior.

A similar trend was observed under both mild (0.5 mA cm^{-2} and 0.5 mAh cm^{-2}) and more aggressive conditions (2 mA cm^{-2} and 2 mAh cm^{-2}) (Fig. 5e, f). GO–PVDF retained relatively stable Coulombic efficiency, while GO–PAA underwent gradual degradation followed by a sharp decline under high-current conditions. This performance gap became increasingly pronounced at high current densities, highlighting the increasing importance of interfacial stability under severe operating conditions. The rate-dependent measurements further support this observation (Fig. 5g). GO–PVDF exhibited gradual performance decay with increasing current density and closely recovered its initial level upon returning to a lower current, whereas GO–PAA demonstrated limited recovery, indicating irreversible interfacial degradation accumulated under high-current operation. Collectively, these electrochemical signatures indicate that GO–PAA exhibits progressive interfacial instability, whereas GO–PVDF maintains a stable interfacial environment even under high Li-ion flux conditions.

The EIS results provide additional insight into these interfacial behaviors (Fig. 5h, i). After the first cycle, GO–PAA exhibited lower resistance values (R_{ohmic} ≈ 8 Ω and R_{ct} ≈ 102 Ω) than GO–PVDF, which can be attributed to enhanced initial interfacial contact due to rapid electrolyte infiltration. However, after 100 cycles, GO–PAA displayed a pronounced increase in resistance (R_{ohmic} ≈ 11 Ω and R_{ct} ≈ 171 Ω), indicating severe interfacial degradation. In contrast, GO–PVDF maintained a lower and more stable R_{ct} with only moderate growth over cycling. Notably, it retained a clear Warburg feature, suggesting the preservation of stable Li-ion transport pathways. These results further imply that GO–PVDF promotes the formation of a more stable and uniform SEI during prolonged cycling.

To clarify the role of GO relative to the binder, Li||Cu half-cell tests were conducted using a PVDF-only coated current collector (Fig. S2). The Only-PVDF exhibited relatively stable Coulombic efficiency during the initial cycles; however, it began to display a noticeable decline after approximately 20 cycles. Conversely, GO–PVDF maintained significantly more stable performance, and the performance gap widened with prolonged cycling. This difference is also reflected in the voltage profiles (Fig. S2b–d). While both samples demonstrated similar behavior in the first cycle, progressive cycling resulted in a clear divergence. The Only-PVDF exhibited increasingly irregular voltage profiles and reduced reversibility, whereas GO–PVDF maintained a stable response. Similar trends are observed under both low and high current densities (Fig. S2g, h), with degradation in the Only-PVDF system becoming more pronounced under high-current conditions.

Further analysis revealed that the Only-PVDF exhibited higher R_{ohmic} (Fig. S2i). This can be attributed to its low electrical conductivity and limited interaction with the electrolyte, which results in non-uniform interfacial contact. In contrast, GO–PVDF enabled more uniform Li nucleation through the oxygen-containing functional groups in GO while maintaining strong adhesion at the interface, thereby facilitating the formation of a stable SEI and homogeneous Li deposition. These observations highlight a synergistic effect between GO and PVDF, where GO contributes to interfacial uniformity, and PVDF provides mechanical robustness. Taken together, these findings demonstrate that although wettability enhances initial interfacial kinetics, long-term electrochemical performance is primarily governed by the maintenance of structural integrity and interfacial stability during repeated cycling.

View Article Online
DOI: 10.1039/D6NR01899H

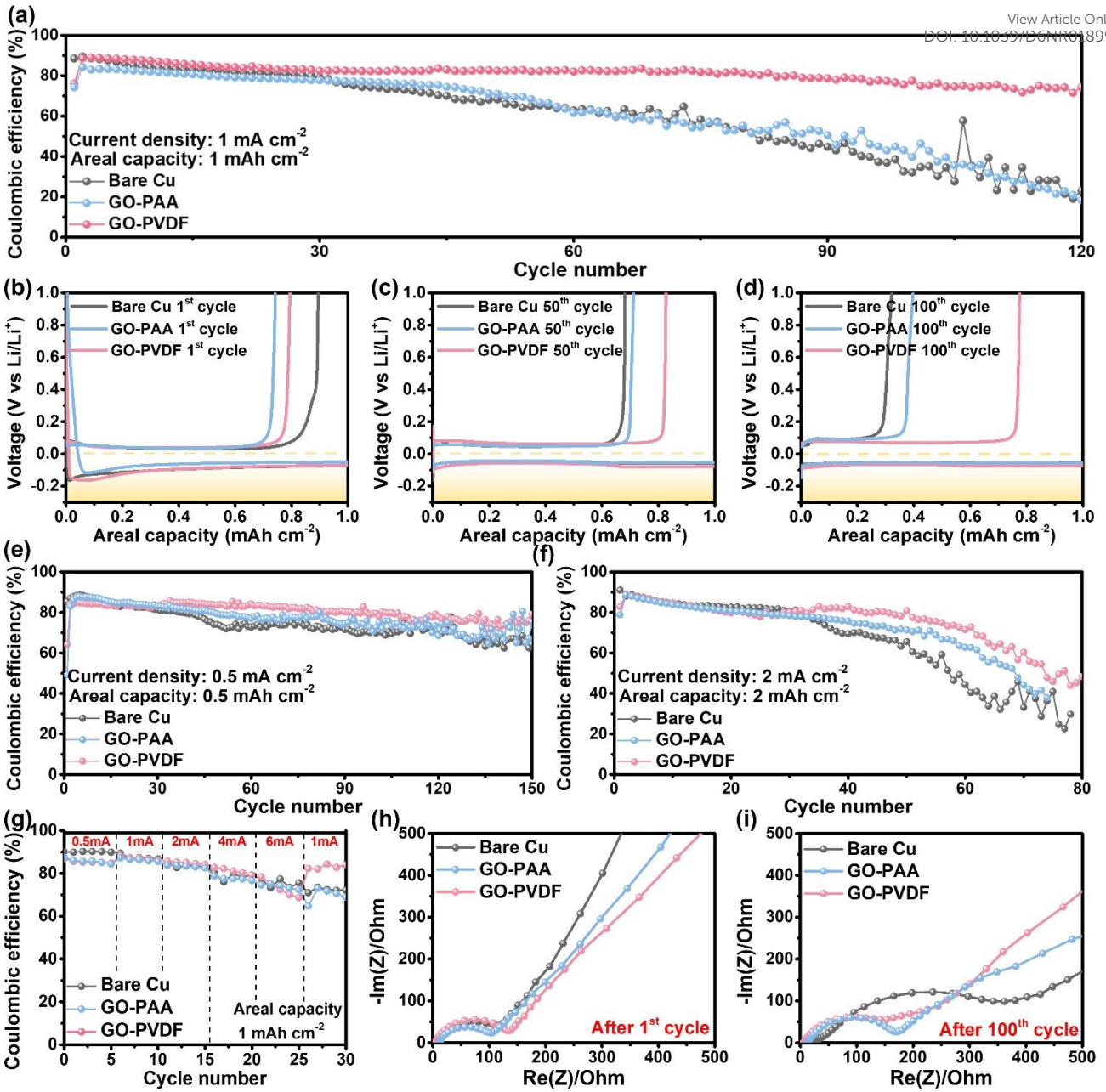

Fig. 5 (a) Cycling performance of Li||Cu half cells employing the bare Cu, GO–PAA, and GO–PVDF at a current density of 1.0 mA cm^{-2} and an areal capacity of 1.0 mAh cm^{-2}. (b–d) Galvanostatic charge–discharge profiles at the 1st, 50th, and 100th cycles. Cycling performance at (e) 0.5 mA cm^{-2} with 0.5 mAh cm^{-2} and (f) 2.0 mA cm^{-2} with 2.0 mAh cm^{-2}. (g) Rate capability of the cells. EIS spectra acquired after (h) the 1st cycle and (i) the 100th cycle.

View Article Online
DOI: 10.1039/D6NR01899H

After 100 cycles of Li plating/stripping at 1 mA cm^{-2} with an areal capacity of 1 mAh cm^{-2}, the surface morphologies of the current collectors were examined (Fig. 6a–d). The bare Cu exhibited a thick and uneven accumulation of dead Li across the entire surface, indicative of severe interfacial degradation caused by nonuniform Li deposition and continuous SEI breakdown and reformation (Fig. 6a). Similarly, the Gr–PVDF was largely covered with dead Li (Fig. 6b), suggesting that the coating layer fails to maintain sufficient interfacial adhesion and structural integrity during prolonged cycling.

Conversely, both GO–PAA and GO–PVDF exhibited significantly reduced dead Li accumulation (Fig. 6c, d), suggesting that GO-based coatings promote more uniform Li nucleation at the initial stage. However, their long-term structural stability differed markedly. These differences can be clearly observed in the SEM images (Fig. 6e–l). The bare Cu exhibited irregular and sharp dendritic structures due to localized current concentration and heterogeneous Li growth (Fig. 6e, i). The characteristic Li width was measured to be 0.61 µm (Table S1), corresponding to thin Li structures. Consistent with this morphology, the charge-transfer resistance increased significantly from 113 Ω after the first cycle to 381 Ω after 100 cycles, indicating severe interfacial degradation during prolonged cycling. Gr–PVDF showed a similar morphology with pronounced dendritic features (Fig. 6f, j), indicating that the initial interfacial modification effect is progressively lost due to interfacial degradation during cycling. Notably, the initial Li deposition morphology of Gr–PVDF was relatively uniform (Fig. S3), indicating that uniform initial Li deposition alone does not necessarily guarantee stable long-term cycling performance. This interpretation is further supported by quantitative morphology analysis. The characteristic Li width of Gr–PVDF was measured to be 1.37 µm (Table S1), while the charge-transfer resistance increased from 36 Ω to 175 Ω during cycling, suggesting that the initially improved Li deposition environment could not be effectively maintained due to progressive interfacial degradation.

Although GO–PAA partially suppressed dendrite formation, its surface appeared relatively loose and nonuniform, with localized structural collapse observed in several regions (Fig. 6g, k). This behavior is attributed to electrolyte-induced swelling, which disrupts coating continuity and weakens interfacial adhesion during repeated cycling. Such structural instability leads to the gradual loss of interfacial regulation capability. The characteristic Li width of GO–PAA was measured to be 1.28 µm (Table S1), which is comparable to that of Gr–PVDF. Nevertheless, the coating exhibited noticeable structural instability after prolonged cycling, indicating that maintaining coating integrity is equally important for preserving stable Li growth. In contrast, GO–PVDF maintained a dense, continuous, and compact morphology even after prolonged cycling (Fig. 6h, l), effectively suppressing dendritic Li growth and minimizing surface roughening. Consistent with the relatively uniform initial Li deposition morphology observed in Fig. S3, GO–PVDF retained a homogeneous morphology after 100 cycles, suggesting that its mechanically robust and strongly adhered coating layer effectively preserves the initially established uniform deposition environment during repeated Li plating/stripping processes. Notably, GO–PVDF exhibited the largest characteristic Li width of 2.27 µm (Table S1) while showing the smallest increase in charge-transfer resistance, from 134 Ω to 142 Ω. The larger characteristic Li width does not indicate more severe dendritic growth. Rather, it reflects a laterally expanded and homogeneous Li deposition morphology, in which Li grows across the current collector surface to form broad and compact deposits instead of localized dendritic structures. Such Li growth is expected to mitigate localized current concentration and suppress continuous SEI reconstruction, thereby contributing to improved interfacial stability during prolonged cycling.

The corresponding schematic summarizes these distinct behaviors (Fig. 6m–p). Bare Cu suffers from localized Li growth and dendrite formation due to nonuniform nucleation and unstable SEI. Gr–PVDF initially facilitates Li deposition but undergoes interfacial delamination, which results in unstable growth. GO–PAA exhibits improved wettability but experiences structural degradation due to electrolyte-induced swelling. In contrast, GOfi–PVDF achieves both uniform Li nucleation and stable interfacial retention, resulting in homogeneous Li growth and a stable SEI environment. These observations establish a direct correlation between morphological evolution and electrochemical performance, underscoring that long-term stability is governed not solely by initial nucleation behavior but primarily by the ability of the buffer layer to maintain mechanical integrity and interfacial adhesion under repeated cycling.

View Article Online
DOI: 10.1039/D6NR01899H

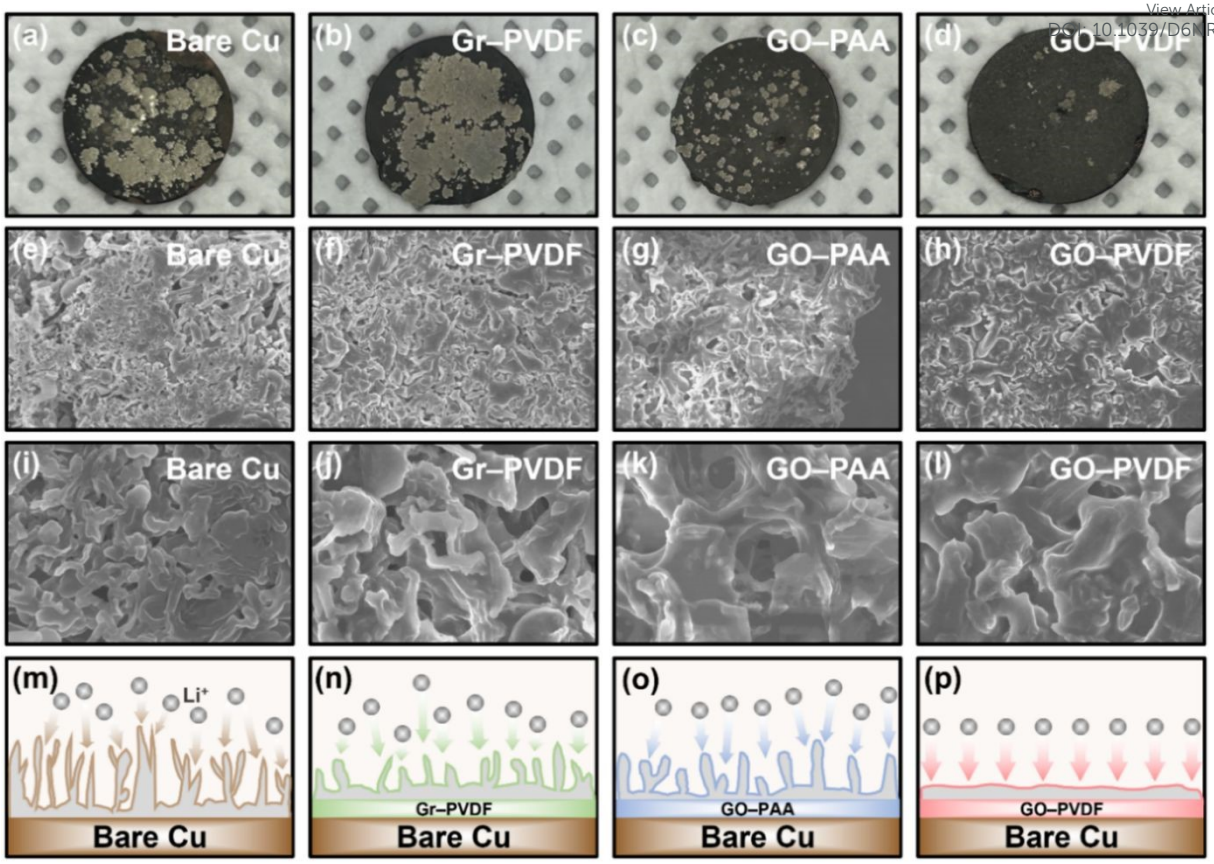

Fig. 6 (a–d) Optical images of the bare Cu, Gr–PVDF, GO–PAA, and GO–PVDF after 100 cycles of Li plating/stripping at 1 mA cm^{-2} with an areal capacity of 1 mAh cm^{-2}. (e–h) Low-magnification and (i–l) high-magnification SEM images of the samples. (m–p) Schematic illustrations of Li growth behavior on each current collector.

To elucidate the origin of the distinct interfacial behaviors, XPS depth profiling analysis was performed to examine the depth-dependent SEI composition on the bare Cu and GO–PVDF. After 30 cycles at 1 mA cm^{-2} and an areal capacity of 1 mAh cm^{-2}, followed by additional Li deposition, the surface chemical composition was analyzed as a function of etching depth.

The C 1s spectra of bare Cu exhibited dominant peaks corresponding to C=O, C–O, and C–C/C–H species, along with a noticeable Li_2CO_3 component at the surface (Fig. 7a).[56] Notably, the persistent Li_2CO_3 after etching indicates that carbonate-based decomposition products extend deep into the SEI layer. This observation reflects the formation of a thick and compositionally heterogeneous SEI associated with continuous electrolyte decomposition.[57] Furthermore, the variation in peak intensities with etching depth confirms the existence of significant compositional heterogeneity throughout the SEI. In contrast, GO–PVDF displayed a dominant C–O peak attributed to the oxygen-containing functional groups in GO, while the relative fraction of Li_2CO_3 was significantly lower (Fig. 7b). Importantly, the spectral features remained largely unchanged upon etching, indicating a consistent SEI composition along the depth direction.

A similar trend was observed in the O 1s spectra. For bare Cu, C–O and $ROCO_2Li$ species dominated near the surface, whereas Li_2CO_3 and Li_2O became increasingly prominent with depth (Fig. 7c). This depth-dependent evolution is consistent with the formation of a stratified and compositionally evolving SEI structure. However, GO–PVDF exhibited relatively stable distributions of $ROCO_2Li$ and Li_2CO_3 across the depth (Fig. 7d), confirming the presence of a chemically uniform SEI.[58]

The F 1s spectra further highlight this distinction. In bare Cu, Li_xPF_y species were present near the surface, while LiF became dominant in the inner SEI region (Fig. 7e), indicating progressive electrolyte decomposition and continuous SEI reconstruction during cycling.[33] In contrast, GO–PVDF exhibited LiF as the dominant component across the SEI depth (Fig. 7f). This uniform LiF-rich interphase is known to provide high mechanical strength and chemical stability while facilitating efficient Li-ion transport, thereby enhancing interfacial stability.[59] Overall, these results demonstrate that bare Cu forms a compositionally stratified and dynamically evolving SEI, whereas GO–PVDF promotes the formation of a uniform and LiF-rich interphase with minimal depth-dependent variation. Such a stable SEI suppresses continuous electrolyte decomposition and mitigates interfacial degradation during repeated cycling, which directly accounts for the improved electrochemical performance of GO–PVDF. This finding highlights that long-term stability is determined not by initial lithiophilicity alone but by the ability of the coating to maintain a uniform and mechanically robust SEI under repeated Li plating/stripping.

View Article Online
DOI: 10.1039/D6NR01899H

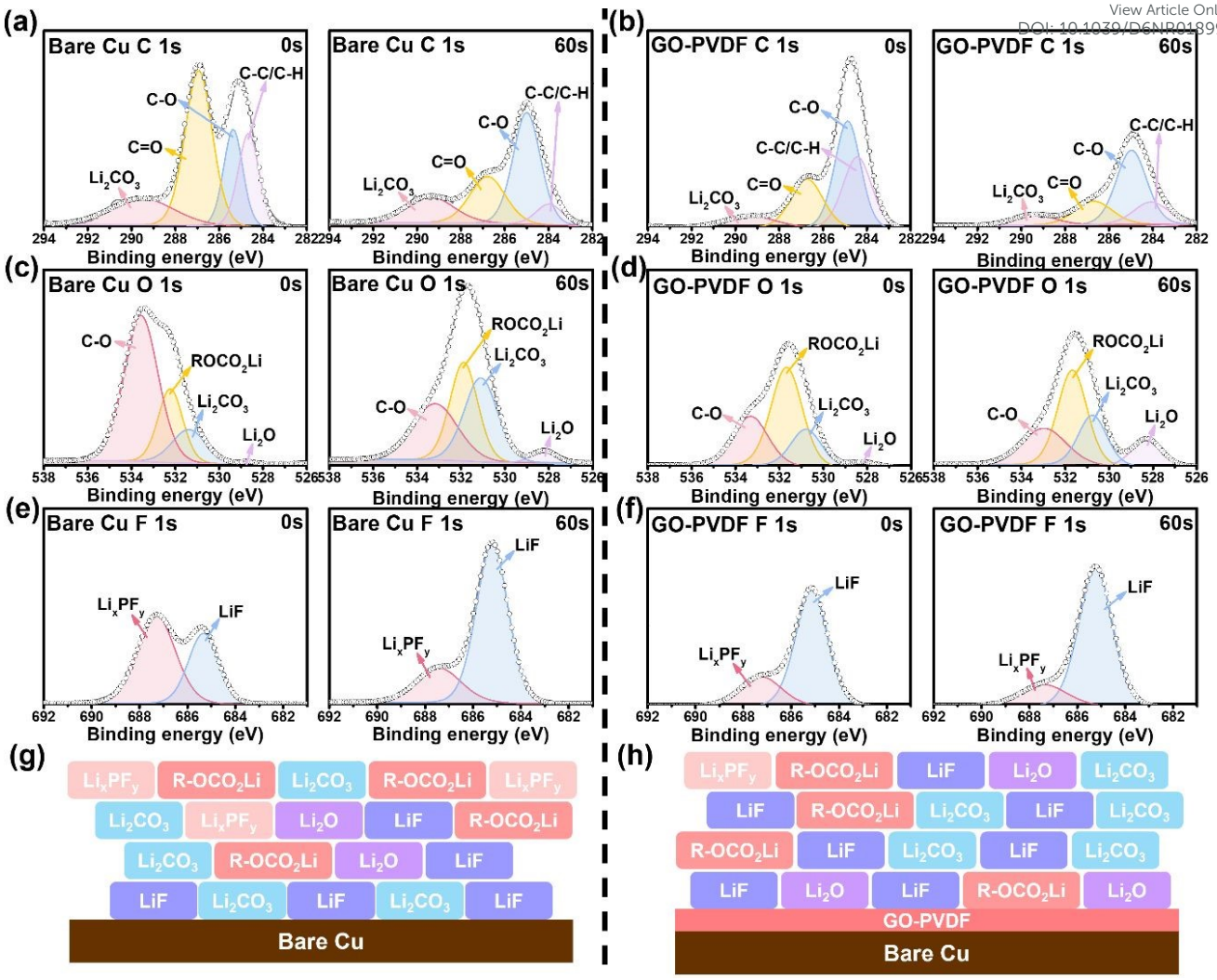

Fig. 7 (a, b) C 1s, (c, d) O 1s, and (e, f) F 1s XPS spectra of bare Cu and GO–PVDF at etching times of 0 and 60 s. (g, h) Schematic illustrations of the SEI structures formed on the bare Cu and GO–PVDF current collectors.

Conclusion

This study elucidates that interfacial stability in current collectors is the key factor governing the long-term electrochemical performance of LMBs. Although uniform initial Li nucleation and enhanced wettability are generally considered beneficial, the findings demonstrate that these factors alone are insufficient to ensure stable cycling behavior. As observed, the GO–PVDF exhibits strong interfacial adhesion and mechanical robustness at the current collector interface, effectively suppressing interfacial degradation and maintaining structural integrity during repeated Li plating/stripping. Consequently, uniform Li deposition is sustained, while localized growth and dead Li formation are significantly mitigated. In contrast, the Gr-PVDF undergoes interfacial degradation due to poor adhesion to the current collector, whereas the GO–PAA system suffers from structural instability induced by electrolyte swelling. These differences indicate that interfacial stability, governed by mechanical robustness and interfacial adhesion, plays a more dominant role in reversible Li plating/stripping than initial interfacial affinity or wettability. XPS depth profiling further revealed that GO–PVDF promotes the formation of a uniform and LiF-rich SEI, whereas bare Cu develops a stratified SEI associated with continuous electrolyte decomposition. This stable SEI suppresses interfacial degradation and contributes to improved electrochemical stability. Overall, these findings provide key insight into the design of interface-engineered current collectors for LMBs, highlighting that long-term performance is governed by not only initial nucleation behavior but also the ability of the coating layer to maintain a mechanically robust and stable interface under repeated cycling.

CRediT authorship contribution statement

Yujin Lee and **Wootaek Choi** contributed equally to this work.

Yujin Lee: Writing – original draft, Investigation, Visualization, Formal analysis, Data curation. **Wootaek Choi:** Writing – original draft, Visualization, Data curation. **Sujeong Woo:**

Methodology, Data curation. **Yeonseo Cho and Geunah Lim:** Formal analysis, Data curation. **Jin Joo:** Formal analysis. **Kyung Rok Han:** Data curation. **In Woo Cheong:** Conceptualization, Formal analysis. **Dongsoo Lee:** Writing – review & editing, Resources, Project administration. **Junghyun Choi:** Writing – review & editing, Resources, Project administration. **Patrick Joohyun Kim:** Supervision, Resources, Writing – review & editing, Validation, Project administration, Conceptualization.

Conflict of Interest

The authors declare no conflict of interest.

Acknowledgements

This work was supported by the National Research Foundation of Korea (NRF) grant funded by the Korean government (MSIT) (RS-2025-16065458 and RS-2025-02217276). This research was supported by the Korea Institute for Advancement of Technology (KIAT), funded by the Ministry of Trade, Industry and Energy (MI) (RS-2024-00419967). This work was also supported by the Industrial Technology Innovation Program (RS-2024-00446635) funded by the Ministry of Trade, Industry & Resources (MOTIR, Korea) and Korea Institute of Industrial Technology Evaluation and Planning (KEIT).

References

1. J. Xie and Y.-C. Lu, Nature communications, 2020, 11, 2499.
2. J. B. Goodenough and K.-S. Park, Journal of the American Chemical Society, 2013, 135, 1167-1176.
3. D. Lin, Y. Liu and Y. Cui, Nature nanotechnology, 2017, 12, 194-206.
4. J. Liu, Z. Bao, Y. Cui, E. J. Dufek, J. B. Goodenough, P. Khalifah, Q. Li, B. Y. Liaw, P. Liu and A. Manthiram, Nature Energy, 2019, 4, 180-186.
5. Z. A. Ghazi, Z. Sun, C. Sun, F. Qi, B. An, F. Li and H. M. Cheng, Small, 2019, 15, 1900687.
6. X.-B. Cheng, R. Zhang, C.-Z. Zhao and Q. Zhang, Chemical reviews, 2017, 117, 10403-10473.
7. Q. Liu, C. Du, B. Shen, P. Zuo, X. Cheng, Y. Ma, G. Yin and Y. Gao, RSC advances, 2016, 6, 88683-88700.
8. W. Xu, J. Wang, F. Ding, X. Chen, E. Nasybulin, Y. Zhang and J.-G. Zhang, Energy & Environmental Science, 2014, 7, 513-537.
9. K. N. Wood, E. Kazyak, A. F. Chadwick, K.-H. Chen, J.-G. Zhang, K. Thornton and N. P. Dasgupta, ACS central science, 2016, 2, 790-801.
10. A. Kushima, K. P. So, C. Su, P. Bai, N. Kuriyama, T. Maebashi, Y. Fujiwara, M. Z. Bazant and J. Li, Nano energy, 2017, 32, 271-279.
11. D. Aurbach, E. Zinigrad, Y. Cohen and H. Teller, Solid state ionics, 2002, 148, 405-416.
12. E. Peled and S. Menkin, Journal of The Electrochemical Society, 2017, 164, A1703-A1719.
13. G. Lu, J. Nai, D. Luan, X. Tao and X. W. Lou, Science Advances, 2023, 9, eadf1550.
14. B. Zhou, A. Bonakdarpour, I. Stoševski, B. Fang and D. P. Wilkinson, Progress in Materials Science, 2022, 130, 100996.
15. W. Choi, M. S. Kang, K. Kim, H. U. Lee, S. B. Cho, J. Choi and P. J. Kim, Nano Energy, 2025, 111444.
16. A. Fu, C. Wang, J. Peng, M. Su, F. Pei, J. Cui, X. Fang, J. F. Li and N. Zheng, Advanced Functional Materials, 2021, 31, 2009805.
17. J. Kim, G. R. Lee, R. B. K. Chung, P. J. Kim and J. Choi, Energy Storage Materials, 2023, 61, 102899.
18. W. Choi, Y. Lee, D. U. Woo, S. Woo, J. Seo, K. Lee, Y. Jung, T. Kim and P. J. Kim, Carbon, 2026, 121448.
19. Q. Yun, Y.-B. He, W. Lv, Y. Zhao, B. Li, F. Kang and Q.-H. Yang, Advanced Materials (Deerfield Beach, Fla.), 2016, 28, 6932-6939.
20. Y. Zhang, W. Luo, C. Wang, Y. Li, C. Chen, J. Song, J. Dai, E. M. Hitz, S. Xu and C. Yang, Proceedings of the National Academy of Sciences, 2017, 114, 3584-3589.
21. S. T. Oyakhire and S. F. Bent, Energy Advances, 2024, 3, 108-122.
22. A. Hu, W. Chen, X. Du, Y. Hu, T. Lei, H. Wang, L. Xue, Y. Li, H. Sun and Y. Yan, Energy & Environmental Science, 2021, 14, 4115-4124.
23. C. Niu, H. Lee, S. Chen, Q. Li, J. Du, W. Xu, J.-G. Zhang, M. S. Whittingham, J. Xiao and J. Liu, Nature Energy, 2019, 4, 551-559.
24. K. Yan, Z. Lu, H.-W. Lee, F. Xiong, P.-C. Hsu, Y. Li, J. Zhao, S. Chu and Y. Cui, Nature Energy, 2016, 1, 16010.
25. X. Wang, R. Kerr, F. Chen, N. Goujon, J. M. Pringle, D. Mecerreyes, M. Forsyth and P. C. Howlett, Advanced Materials, 2020, 32, 1905219.
26. Q. Li, S. Zhu and Y. Lu, Advanced Functional Materials, 2017, 27, 1606422.

27. P. Zhai, L. Liu, X. Gu, T. Wang and Y. Gong, Advanced Energy Materials, 2020, 10, 2001257.
28. M. D. Tikekar, S. Choudhury, Z. Tu and L. A. Archer, Nature Energy, 2016, 1, 1-7.
29. Z. Yu, Y. Cui and Z. Bao, Cell Reports Physical Science, 2020, 1.
30. H. Wu, H. Jia, C. Wang, J. G. Zhang and W. Xu, Advanced Energy Materials, 2021, 11, 2003092.
31. X. Shan, Y. Zhong, L. Zhang, Y. Zhang, X. Xia, X. Wang and J. Tu, The Journal of Physical Chemistry C, 2021, 125, 19060-19080.
32. S. Li, M. Jiang, Y. Xie, H. Xu, J. Jia and J. Li, Advanced materials, 2018, 30, 1706375.
33. K. Xu, Chemical reviews, 2004, 104, 4303-4418.
34. D. Lin, Y. Liu, Z. Liang, H.-W. Lee, J. Sun, H. Wang, K. Yan, J. Xie and Y. Cui, Nature nanotechnology, 2016, 11, 626-632.
35. J. Song, M. Zhou, R. Yi, T. Xu, M. L. Gordin, D. Tang, Z. Yu, M. Regula and D. Wang, Advanced functional materials, 2014, 24, 5904-5910.
36. K. Yan, H.-W. Lee, T. Gao, G. Zheng, H. Yao, H. Wang, Z. Lu, Y. Zhou, Z. Liang and Z. Liu, Nano letters, 2014, 14, 6016-6022.
37. D. Li, M. B. Müller, S. Gilje, R. B. Kaner and G. G. Wallace, Nature nanotechnology, 2008, 3, 101-105.
38. K. Kwon, J. Kim, K. Roh, P. J. Kim and J. Choi, Electrochemistry Communications, 2023, 157, 107598.
39. L. Zhong, Y. Sun, K. Shen, F. Li, H. Liu, L. Sun and D. Xie, Small, 2024, 20, 2407297.
40. I. Kovalenko, B. Zdyrko, A. Magasinski, B. Hertzberg, Z. Milicev, R. Burtovyy, I. Luzinov and G. Yushin, Science, 2011, 334, 75-79.
41. S.-L. Chou, Y. Pan, J.-Z. Wang, H.-K. Liu and S.-X. Dou, Physical Chemistry Chemical Physics, 2014, 16, 20347-20359.
42. M. Park, S. Woo, J. Seo, J. Choi, E. Jeong and P. J. Kim, Electrochimica Acta, 2024, 495, 144426.
43. J. Lopez, A. Pei, J. Y. Oh, G.-J. N. Wang, Y. Cui and Z. Bao, Journal of the American Chemical Society, 2018, 140, 11735-11744.
44. C. Brissot, M. Rosso, J.-N. Chazalviel and S. Lascaud, Journal of power sources, 1999, 81, 925-929.
45. C. Fang, J. Li, M. Zhang, Y. Zhang, F. Yang, J. Z. Lee, M.-H. Lee, J. Alvarado, M. A. Schroeder and Y. Yang, Nature, 2019, 572, 511-515.
46. Z. Liang, D. Lin, J. Zhao, Z. Lu, Y. Liu, C. Liu, Y. Lu, H. Wang, K. Yan and X. Tao, Proceedings of the National Academy of Sciences, 2016, 113, 2862-2867.
47. Q. Pang, X. Liang, C. Y. Kwok and L. F. Nazar, Nature Energy, 2016, 1, 1-11.
48. A. C. Ferrari and J. Robertson, Physical review B, 2000, 61, 14095.
49. C. K. Chua and M. Pumera, Chemical Society Reviews, 2014, 43, 291-312.
50. D. A. Dikin, S. Stankovich, E. J. Zimney, R. D. Piner, G. H. Dommett, G. Evmenenko, S. T. Nguyen and R. S. Ruoff, Nature, 2007, 448, 457-460.
51. K. S. Novoselov, A. K. Geim, S. V. Morozov, D.-e. Jiang, Y. Zhang, S. V. Dubonos, I. V. Grigorieva and A. A. Firsov, science, 2004, 306, 666-669.
52. J. Christensen and J. Newman, Journal of Solid State Electrochemistry, 2006, 10, 293-319.
53. B. Horstmann, J. Shi, R. Amine, M. Werres, X. He, H. Jia, F. Hausen, I. Cekic-Laskovic, S. Wiemers-Meyer and J. Lopez, Energy & Environmental Science, 2021, 14, 5289-5314.
54. T. Foroozan, F. A. Soto, V. Yurkiv, S. Sharifi-Asl, R. Deivanayagam, Z. Huang, R. Rojaee, F. Mashayek, P. B. Balbuena and R. Shahbazian-Yassar, Advanced Functional Materials, 2018, 28, 1705917.
55. A. K. Geim and K. S. Novoselov, Nature materials, 2007, 6, 183-191.
56. K. Xu, Chemical reviews, 2014, 114, 11503-11618.
57. A. Wang, S. Kadam, H. Li, S. Shi and Y. Qi, NPJ Computational materials, 2018, 4, 15.
58. Y. Li, W. Huang, Y. Li, A. Pei, D. T. Boyle and Y. Cui, Joule, 2018, 2, 2167-2177.
59. Y. Lu, Z. Tu and L. A. Archer, Nature materials, 2014, 13, 961-969.

View Article Online
DOI: 10.1039/D6NR01899H

Data Availability Statement

The data supporting the findings of this study are available within the article and its Supplementary Information files. Additional data are available from the corresponding author upon reasonable request.